# Medial Prefrontal–Medial Temporal Theta Phase Coupling in Dynamic Spatial Imagery

Raphael Kaplan[1,2*], Daniel Bush[1*], James A. Bisby[1], Aidan J. Horner[1,3]
Sofie S. Meyer[1], and Neil Burgess[1]

## Abstract

■ Hippocampal–medial prefrontal interactions are thought to play a crucial role in mental simulation. Notably, the frontal midline/medial pFC (mPFC) theta rhythm in humans has been linked to introspective thought and working memory. In parallel, theta rhythms have been proposed to coordinate processing in the medial temporal cortex, retrosplenial cortex (RSc), and parietal cortex during the movement of viewpoint in imagery, extending their association with physical movement in rodent models. Here, we used noninvasive whole-head MEG to investigate theta oscillatory power and phase-locking during the 18-sec postencoding delay period of a spatial working memory task, in which participants imagined previously learned object sequences either on a blank background (object maintenance), from a first-person view-point in a scene (static imagery), or moving along a path past the objects (dynamic imagery). We found increases in 4- to 7-Hz theta power in mPFC when comparing the delay period with a preencoding baseline. We then examined whether the mPFC theta rhythm was phase-coupled with ongoing theta oscillations elsewhere in the brain. The same mPFC region showed significantly higher theta phase coupling with the posterior medial temporal lobe/RSc for dynamic imagery versus either object maintenance or static imagery. mPFC theta phase coupling was not observed with any other brain region. These results implicate oscillatory coupling between mPFC and medial temporal lobe/RSc theta rhythms in the dynamic mental exploration of imagined scenes. ■

## INTRODUCTION

Our capacity to imagine spatially cohesive representations is associated with the medial pFC (mPFC) and medial temporal lobe (MTL) regions such as the hippocampus (Schacter et al., 2012; Schacter & Addis, 2007; Hassabis, Kumaran, Vann, & Maguire, 2007; Burgess, Becker, King, & O'Keefe, 2001). Increases in approximately 4- to 8-Hz mPFC oscillatory power, known as the frontal midline theta rhythm, are observed during internally generated behaviors such as abstract thinking and meditation (Aftanas & Golocheikine, 2001; Sasaki et al., 1996; Lehmann, Henggeler, Koukkou, & Michel, 1993; Banquet, 1973). Notably, there is growing evidence that the frontal midline theta rhythm is also implicated in working and episodic memory function (see Hsieh & Ranganath, 2014, for a recent review).

In parallel, hippocampal theta oscillations in the MTL have been hypothesized to serve as a network hub (Battaglia, Benchenane, Sirota, Pennartz, & Wiener, 2011) and global signal integrator (O'Keefe, 2006) for information from neocortical regions, including the mPFC and medial parietal/retrosplenial (RSc) cortices. The hippocampal theta rhythm is strongly associated with translational movement in rodents (O'Keefe & Nadel, 1978;

Vanderwolf, 1969) but has also been observed in the human MTL and several neocortical areas including the mPFC and the medial parietal lobe/RSc during virtual navigation (Kaplan et al., 2012; Ekstrom et al., 2005; Caplan et al., 2003; Kahana, Sekuler, Caplan, Kirschen, & Madsen, 1999). Recently, several studies have found increased theta phase coupling between these regions during spatial and autobiographical memory retrieval (Fuentemilla, Barnes, Duzel, & Levine, 2014; Kaplan et al., 2014; Foster, Kaveh, Dastjerdi, Miller, & Parvizi, 2013; Watrous, Tandon, et al., 2013), but whether theta power or phase coupling contributes to spatial imagery is currently unclear.

This issue is addressed by a speculative neural level model of memory-guided visuospatial imagery (Bird & Burgess, 2008; Byrne, Becker, & Burgess, 2007; Burgess et al., 2001). It proposes that the MTL provides allocentric scene information consistent with a single viewpoint location and that this information is translated, via intermediate representations in the RSc, into an egocentric image consistent with a specific viewing direction, supported in a medial parietal "window" (PW). This "top–down" activation of the PW from MTL occurs during the first half of each theta cycle, whereas "bottom–up" updating of the MTL representation from the PW representation occurs in the second half of each cycle—allowing egocentric manipulations in the PW to propagate back

---

[1]University College London, [2]Universitat Pompeu Fabra, Barcelona, Spain, [3]University of York
*Authors contributed equally to this work.

to the MTL. These egocentric manipulations include se-
lective attention to specific scene elements (allowing re-
activation of their identity/perceptual properties in the
MTL) and spatial updating because of the real or imag-
ined movement of viewpoint.

According to this model, during actual movement, at
the start of a theta cycle, motor efference copy from pre-
motor areas (Graziano & Gross, 1993) drives egocentric
spatial updating of locations by modifying the allocentric-
to-egocentric translation to accommodate the effect of
the movement. The updated egocentric representation
then feeds back to update MTL representations during
the second half of the theta cycle. The model proposes
that the imagined movement of viewpoint (dynamic im-
agery) occurs in the same way, driven by mock motor
efference copy from pFC, which could be used in behav-
iors like planning. The theta rhythmicity associated with
prefrontal control of working memory maintenance

(Hsieh & Ranganath, 2014) would thus have to synchro-
nize with the theta-modulated MTL–PW interaction so as
to be able to direct dynamic imagery. However, we are
unaware of any attempts to investigate theta rhythmicity
or phase coupling during dynamic imagery.

Using a spatial working memory task with noninvasive
whole-head MEG, we tested this prediction. In the exper-
iment, participants encoded the location of five objects
overlaid on a scene or blank background (Figure 1). Par-
ticipants then closed their eyes during a 20-sec eyes-
closed delay period and imagined previously learned
object sequences either overlaid on a blank background
(object maintenance; Figure 1A), from a static first-person
viewpoint in a scene (static imagery; Figure 1B), or moving
along a path past the objects (dynamic imagery; Figure 1C).
Afterward, participants were prompted to sequentially
match each object to its respective location on the screen,
in the scene, or along the path.
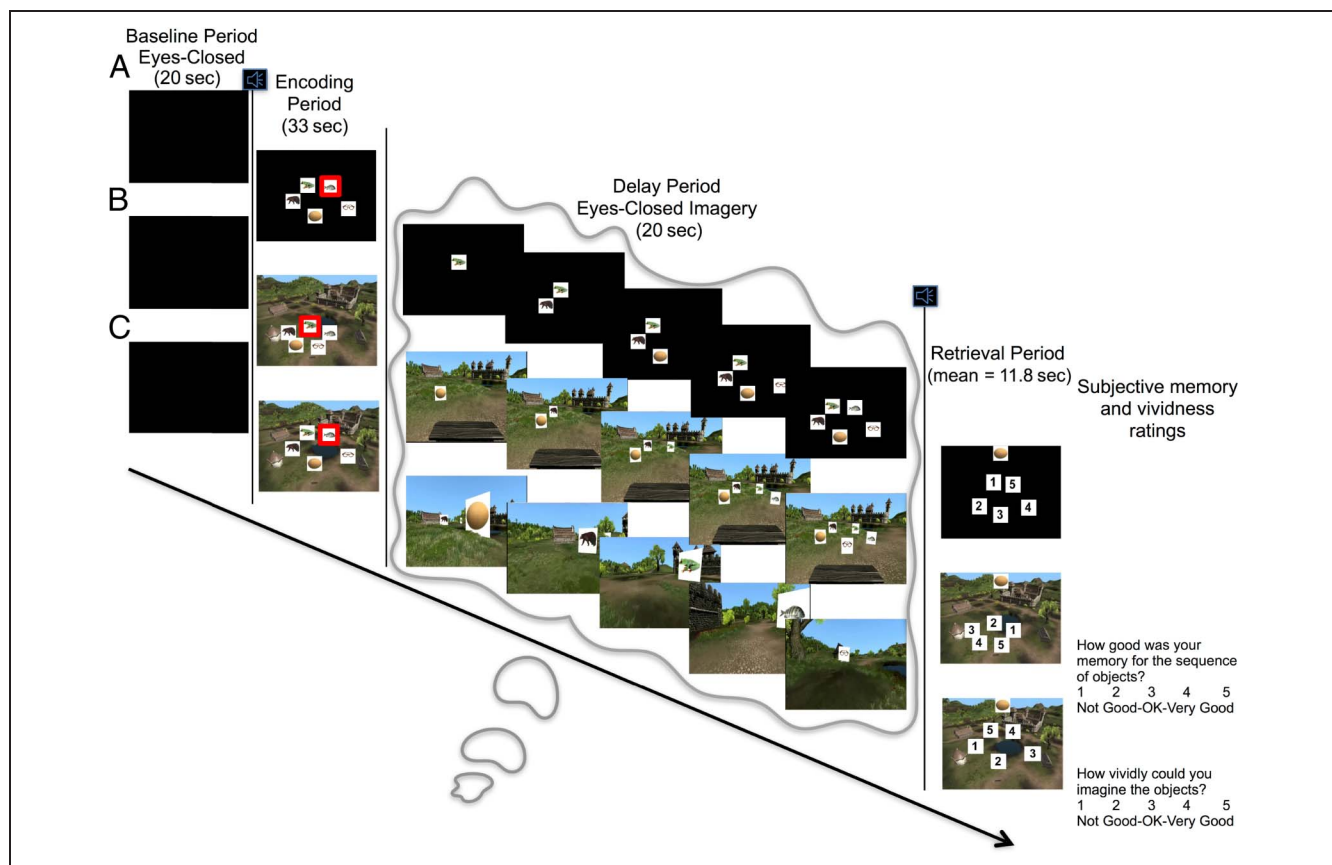


**Figure 1.** Experiment trial structure. After a 20-sec eyes-closed baseline period, an auditory tone alerted the participants to an upcoming
encoding period (for all trial types). These encoding periods fell into one of three conditions. (A) Object maintenance: Participants were presented
with a set of objects overlaid on a black background and instructed to maintain a memory of those object locations during a 20-sec eyes-closed
delay period. (B) Static imagery: Participants were presented with a set of objects overlaid on a static scene and instructed to maintain a
memory of those object locations from an imagined first-person viewpoint sitting on the bench set within each scene during a 20-sec eyes-closed
delay period. (C) Dynamic imagery: Participants were presented with a set of objects overlaid on a static scene and instructed to maintain a
memory of those object locations from a first-person viewpoint as they imagined moving through the scene on a trajectory that sequentially
passed each object during a 20-sec eyes-closed delay period. After the delay period, participants were prompted with an image of each object
and asked to identify its previous location at their own pace (mean = 11.8 sec) as well as report their perceived memory performance and
vividness of imagination during the delay period.

We were primarily interested in the potential co-occurrence of frontal midline/mPFC, RSc, and MTL theta oscillations, interregional mPFC theta phase coupling during the delay period, and whether these phenomena would be modulated by the context of the object sequence imagination task (blank, static spatial, or dynamic spatial). We predicted an increase in frontal midline/mPFC theta power during the delay period, because of the demands of working memory function (Hsieh & Ranganath, 2014). In addition, theta phase coupling with MTL and parietal regions, indicating the presence of functional interactions between these regions, would be specifically recruited to dynamically shift viewpoint during spatial imagery. The blank background condition provides a necessary control for the basic working memory components of the task, whereas the static imagery condition provides a control for working memory accompanied by spatial imagery in the absence of imagined movement. Although spatial updating of object locations could be performed egocentrically (Wang & Spelke, 2000; Wang & Simons, 1999), in the context of a spatial scene, the updating of object locations also involves allocentric processing of locations relative to the environment (Burgess, Spiers, & Paleologou, 2004) and thus egocentric–allocentric translation (Burgess, 2006). Thus, we predicted that mPFC–MTL/parietal theta phase locking would specifically increase with dynamic imagery demands.

## METHODS

### Participants

Sixteen participants (seven women; mean age = 22.8 years, $SD$ = 4.07 years) gave written consent and were compensated for performing the experimental task, as approved by the local research ethics committee at the University College London in accordance with the Declaration of Helsinki protocols. All participants were right-handed, had normal or corrected-to-normal vision, and reported to be in good health with no prior history of drug abuse, neurological disease, or psychiatric illness.

### Task

Stimuli were presented via a digital LCD projector (brightness = 1500 lumens, resolution = 1024 × 768 pixels, refresh rate = 60 Hz) onto a screen (height = 32 cm, width = 42 cm, distance from participant = ~70 cm) that was parallel to the participant's face inside a magnetically shielded room using the Cogent (www.vislab.ucl.ac.uk/cogent.php) toolbox running in MATLAB (The MathWorks, Inc., Natick, MA). Participants were fitted with MEG-compatible earbuds to deliver auditory stimuli associated with the experiment.

Participants performed a spatial working memory task in the MEG system, during which they were asked to remember the locations of five different everyday objects

(e.g., bicycle, lemon) framed by an equally sized white square and overlaid on a blank background or scene. Participants first viewed an example video of each condition recorded from a first-person viewpoint with the same sequence of objects, so they would have an idea of what to imagine and the ideal pacing of imagination during each particular delay period. Participants were instructed to repeat imagination of the sequences if they finished imagining a learned sequence before the end of the delay period. Participants then performed a single practice session of the task, before three counterbalanced pseudorandomized sessions lasting approximately 15 min each inside the scanner.

In the task, participants first had a 20-sec baseline period of eyes-closed rest. This was followed by a 3-sec habituation period, during which participants viewed either a blank background or one of four different scenes created using Unity software (Unity Technologies, San Francisco, CA). A different scene was used for each session (dirt surface environment containing a cemetery and small river with a bridge, grassy forest clearing containing walking paths and a church, a beach environment with tents and stranded boats, and for the practice session, a grassy hill environment containing a small pond and castle). Each scene had a bench in the foreground. After the end of the habituation period, participants were sequentially presented with five objects, arranged circularly in different locations over the scene/background. Each new object was highlighted with a red frame and would appear for 3 sec (with a randomized ±0.3-sec jitter) until all objects appeared overlaid on the background. The appearance of each new object was preceded by a blink period, during which the objects and scene were replaced with a fixation point and the word BLINK for 1 sec. This was followed by a 2-sec intertrial interval before the object sequence resumed with another object highlighted with a red frame. Blocks were counterbalanced for starting location and direction of object presentation (clockwise and counterclockwise). Objects were either presented in a larger circle, to give way for a plausible walking path for dynamic imagery, or clustered in a small circle in front of a bench in the foreground for all objects to be visible from a single viewpoint inside the environment. For the object maintenance condition, objects were presented with equal frequency in either large or small circles over a black background. Importantly, there were no significant differences in behavioral memory performance ($t(15)$ = 0.011, $p$ = .992), RTs ($t(15)$ = −1.34, $p$ = .198), subjective memory ($t(15)$ = 0.983, $p$ = .341), or vividness ratings ($t(15)$ = 0.433, $p$ = .671) between trials with objects arranged in large and small circles within this condition.

After the encoding phase of the experiment, participants had a 20-sec delay period. During the delay period, participants received instructions to close their eyes and either imagine sitting and passively view the locations of the objects in the scene from a static position on the bench (static imagery); imagine walking slowly through

the scene, passing each object sequentially (dynamic imagery); or in the case of objects being presented over a black background, simply "remembering the locations of the objects" (object maintenance). They were cued to open their eyes with an auditory tone played into the participants' headphones.

After the auditory tone, the scene/black background from the encoding period was presented again with numbered squares (1–5) superimposed in place of the objects. Participants were then prompted with a picture of each object at the top of the screen and had to match the object to the number of its corresponding location at their own pace. Immediately after the matching of the spatial location for each object, participants had to indicate how good their memory was for that block and how vivid their imagination during the delay period had been on a 1–5 scale, with 1 being very low and 5 being very high.

Participants performed 36 blocks across three sessions, with each of the three conditions being pseudorandomized within a session. Scene order was also counterbalanced across participants. Over the course of the MEG experiment, participants learned 12 different sequences of objects (60 objects in total), once for each of the three conditions and counterbalanced for order.

## MEG Recording and Preprocessing

Data were recorded continuously from 274 axial gradiometers using a CTF Omega (Vancouver) whole-head system at a sampling rate of 600 Hz in third-order gradient configuration. MEG was preferred to EEG in this experiment because of the increased number of recording channels, high signal-to-noise ratio, and reduced setup time. Participants were also fitted with four EOG electrodes to measure vertical and horizontal eye movements. MEG data analysis made use of custom MATLAB scripts, SPM8 (Wellcome Trust Centre for Neuroimaging, London, United Kingdom; Litvak et al., 2011), and Fieldtrip (Oostenveld, Fries, Maris, & Schoffelen, 2011).

For preprocessing, MEG data were epoched into 20-sec baseline periods before the encoding period and during the delay period for each of the three conditions. Trials were visually inspected, with any trial featuring head movement or muscular artifacts being removed, along with any corresponding baseline or task period to allow for consistent trial comparison. After visual inspection, a mean of 32.1 ($SD$ = 6.04) trials from the total of 36 trials in the experiment remained for analysis. This included a mean of 10.7 ($SD$ = 2.5) dynamic imagery trials, 10.6 ($SD$ = 2.19) static imagery trials, and 10.8 ($SD$ = 1.8) object maintenance trials per participant, regardless of trial-by-trial performance. To avoid further physiological artifacts, data were not analyzed until 1 sec after the beginning of eyes-closed maintenance or baseline period and not until 1 sec before the end (i.e., the central 18 sec of the 20-sec delay period).

## MEG Source Reconstruction

The linearly constrained minimum variance (LCMV) scalar beamformer spatial filter algorithm from SPM8 was applied to the raw time series and used to generate source activity maps in a 10-mm grid (Barnes & Hillebrand, 2003). Coregistration to Montreal Neurological Institute coordinates was based on nasion and left and right preauricular fiducial points. The forward model was derived from a single-shell model (Nolte, 2003) fit to the inner skull surface of the inverse normalized SPM template. Previous studies have shown negligible improvements in spatial resolution by fitting MEG data to individual structural MR images, rather than a canonical template image, under realistic levels of error and head movement (Troebinger et al., 2014; Henson, Mattout, Phillips, & Friston, 2009). The beamformer source reconstruction algorithm consists of two stages: first, based on the data covariance and leadfield structure, weights are calculated, which linearly map sensor data to each source location, and second, a summary statistic based on the mean oscillatory power between experimental conditions is calculated for each voxel.

Because of the proximity of frontal midline regions to the eyes, we wished to control for any possible influence of EOG muscular artifacts during the maintenance period on the estimates of oscillatory power. We therefore computed the variance of two simultaneously recorded EOG signals across each delay period, as a proxy for the number of eye movements made during that delay period, and removed any covariance between these EOG variance values and oscillatory power measurements across voxels by linear regression (Kaplan et al., 2014). This left "residual" oscillatory power measurements for all trials whose variance could not be accounted for by changes in the variance of the EOG signal between trials, and these residual values were used as summary images for the subsequent analyses.

In addition to movements in the ocular region, phase coupling measures can be biased by concurrent changes in oscillatory power because of changes in the signal-to-noise ratio (Muthukumaraswamy & Singh, 2011). To control for any possible influence of changes in oscillatory power (or EOG artifacts) on our phase coupling measures, we repeated the control analysis described above, with additional linear regressors corresponding to oscillatory power in seed and source voxels for each trial (Kaplan et al., 2014). Similarly, we constructed linear regressors for four behavioral measures across trials—RT, memory performance (percentage of object locations remembered correctly for a given trial), subjective memory, and vividness ratings—to examine correlations between behavioral performance and phase coupling values across trials in each voxel.

## Phase Coupling

Instantaneous theta phase in voxel $n$ at time $t$, $\emptyset(t, n)$, was extracted from the analytic signal obtained by applying the

Hilbert transform to the 4- to 7-Hz band-pass second-order Butterworth filtered time series generated by the LCMV beamformer algorithm. The mPFC seed voxel for each participant was chosen as that with the greatest power increase between baseline and maintenance periods within 20 mm of the group maximum coordinates to account for observed variance in frontal midline source location among participants (Kaplan et al., 2014; Isihara, Hayashi, & Hishikawa, 1981). First, we used the phase lag index (PLI) to assay theta phase coupling between that single seed voxel and every other voxel in the brain. The PLI is computed by assigning a value of +1 or −1 at each time step according to whether the phase difference between seed and source voxels is positive or negative and then taking the absolute value of the mean over time, which will tend to 0 for randomly distributed phase differences and to 1 for a consistent nonzero phase relationship (Equation 1). The PLI measure is designed to ameliorate volume conduction effects by being increasingly less sensitive to coupling effects as phase differences approach zero (Stam, Nolte, & Daffertshofer, 2007). PLI values for each trial are averaged for each condition before being entered into a second-level statistical analysis:

$$PLI = \frac{1}{T} \left| \sum_{t=1}^{T} sign[\emptyset(t, \text{seed}) - \emptyset(t, n)] \right| \qquad (1)$$

Second, to confirm the robustness of our PLI effects, we conducted a parallel phase coupling analysis using the phase locking value (PLV; Lachaux, Rodriguez, Martiniere, & Varela, 1999). The PLV is computed as the resultant vector length of phase differences at each time point, such that a larger value indicates less variability in the phase difference between two signals over time (Equation 2). As with PLI values, PLV values for each trial are averaged for each condition before being entered into a second-level statistical analysis:

$$PLV = \frac{1}{T} \left| \sum_{t=1}^{T} \exp(i[\emptyset(t, \text{seed}) - \emptyset(t, n)]) \right| \qquad (2)$$

### Statistical Analyses

For a comparison between delay period and baseline condition, summary images for each participant were entered into a one-sample *t* test in SPM8. Regressors for RT, memory performance (percentage of object locations remembered correctly for a given trial), subjective memory, and vividness ratings, in addition to the "nuisance" regressors described above, were each included in the general linear model. For comparisons between conditions, summary images for each participant and each delay period condition (object maintenance, static imagery, and

dynamic imagery) were entered into a second-level 1 × 3 within-participant ANOVA in SPM8.

To address the issue of multiple comparisons, we used family-wise error (FWE) correction, derived from Gaussian Random Field Theory and implemented in SPM8 (Kiebel & Friston, 2004a, 2004b; Worsley, Taylor, Tomaiuolo, & Lerch, 2004; Worsley et al., 1996). To summarize, this approach treats the data, under the null hypothesis, as continuous random fields, where the distribution of the Euler characteristic of any statistical process derived from these fields can be used as an approximation to the null distribution required for inference (Kilner, Kiebel, & Friston, 2005). A peak voxel significance threshold of *p* < .05 FWE-corrected for multiple comparisons across the whole-brain volume was used for the power analyses. For the theta phase coupling analyses, an MTL ROI for small-volume correction (SVC) for multiple comparisons (peak voxel FWE, *p* < .05) was constructed using a bilateral MTL mask encompassing the amygdala, hippocampus, and parahippocampal and lingual gyrus (to conservatively include all of the parahippocampal place area regions that respond to landmark information; Epstein, 2008) from the automated anatomical labeling toolbox for SPM (Tzourio-Mazoyer et al., 2002). All images are displayed at the *p* < .001 uncorrected threshold (cluster extent of at least 20 voxels after interpolation to the Montreal Neurological Institute brain) for illustrative purposes. In addition, only clusters containing a significant peak voxel are displayed.

## RESULTS
### Behavioral Results

Participants remembered an average of 74.7% (standard error = 5.33%) object locations correctly with a mean RT of 1980 msec for matching an individual object to its respective location after the onset of the retrieval period. On a scale of 1–5 (1 being unsatisfactory and 5 being very good), participants rated each working memory trial for subjective vividness (mean = 3.37, standard error = 0.147) and subjective memory (mean = 3.81, standard error = 0.167). There was a significant interaction between Performance and Condition ($F(2, 30) = 5.66$, $p = .016$; Figure 2A), where performance was significantly higher for object maintenance than static imagery ($t(15) = 3.21$, $p = .006$), but not dynamic imagery ($t(15) = 0.715$, $p = .486$). We observed no significant difference between memory performance in static and dynamic imagery conditions ($t(15) = 1.67$, $p = .117$).

During the retrieval period, there was no significant difference in RT when matching objects to their location among the three conditions ($F(2, 30) = 3.30$, $p = .067$; Figure 2B). There was, however, a significant difference in subjective memory ratings by condition ($F(2, 30) = 11.4$, $p = .001$; Figure 2C). Similar to measured memory performance, subjective memory ratings were significantly
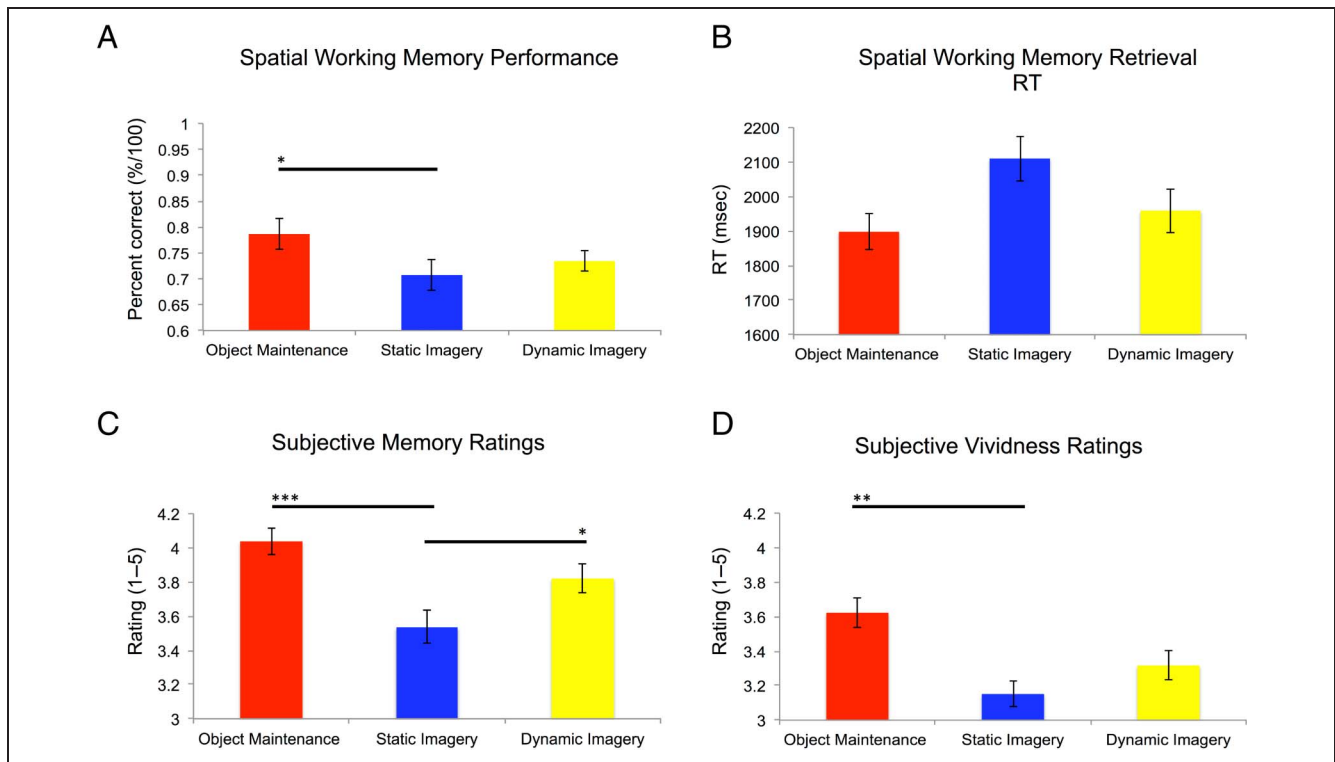
**Figure 2.** Behavioral results. (A) Average trial-by-trial memory performance for each experimental condition during the retrieval phase. Main effect of Condition: $F(2, 30) = 5.66$, $p = .016$. (B) Average trial-by-trial RT during the retrieval phase for Objects 2–5 in the sequence (as retrieval was self-paced and very long RTs were often recorded for Object 1). (C) Average trial-by-trial subjective memory ratings made on a scale of 1–5 (1 = *unsatisfactory*, 5 = *very good*) given immediately after the retrieval phase. Main effect of Condition: $F(2, 30) = 11.4$, $p = .001$. (D) Average trial-by-trial vividness ratings made on a scale of 1–5 (1 = *poor*, 5 = *very good*). Main effect of Condition: $F(2, 30) = 9.42$, $p = .003$. All bar graphs show mean ± *SEM* over the 16 participants. $^*p < .05$; $^{**}p < .005$; $^{***}p < .001$.

higher for object maintenance than static imagery ($t(15) = 4.10$, $p = .001$), but not dynamic imagery trials ($t(15) = 1.54$, $p = .144$). Subjective memory ratings were also higher for dynamic than static imagery trials ($t(15) = 2.58$, $p = .021$). In addition, there was a significant Subjective vividness ratings × Condition interaction ($F(2, 30) = 9.42$, $p = .003$; Figure 2D). Specifically, vividness ratings were significantly higher for object maintenance than static imagery ($t(15) = 3.71$, $p = .002$), but not dynamic imagery trials ($t(15) = 1.71$, $p = .109$). There was no difference in vividness ratings between dynamic and static imagery trials ($t(15) = 1.55$, $p = .143$).

To summarize, performance, subjective memory, and vividness ratings were each significantly higher during object maintenance trials than static imagery trials but not significantly different from dynamic imagery trials, and subjective memory ratings were significantly higher in dynamic imagery trials compared with static imagery trials.

## Theta Power Changes and Source Reconstruction

To assess changes in frontal midline oscillatory power associated with the working memory task, we first extracted low-frequency power spectra for the middle 18 sec of eyes-closed rest (i.e., baseline) and mental imagery of object location (i.e., delay) periods collapsed across all conditions from a 20-mm spherical ROI in source space, centered on frontal midline coordinates identified by a previous study ($x = 0$, $y = 58$, $z = 22$; Kaplan et al., 2014). A comparison of these power spectra identified a prominent increase in theta power between the baseline and delay periods that peaked at ~5.5 Hz (Figure 3A). We subsequently defined our frontal midline theta band of interest as a 3-Hz frequency window centered on this peak (i.e., 4–7 Hz). As expected, an examination of changes in 4- to 7-Hz power at the sensor level showed a large increase between the baseline and delay periods over fronto-temporal regions (Figure 3B).

Next, we utilized the LCMV beamformer algorithm (Barnes & Hillebrand, 2003) to estimate all cortical sources that exhibited significant increases in 4- to 7-Hz theta power between the baseline and delay periods. We identified a single large cluster peaking in the mPFC (peak at $x = 22$, $y = 50$, $z = 0$; $t(15) = 6.76$; $z$ score = 4.51; peak voxel FWE whole-brain corrected, $p = .012$; Figure 3C), extending into the right anterior temporal lobe/MTL. Using a $1 \times 3$ within-participant repeated-measures ANOVA by condition, we did not observe any significant theta power differences between conditions. Furthermore, we observed no correlations between theta power and performance, retrieval phase RT, participant memory ratings, or vividness ratings over trials. In addition,
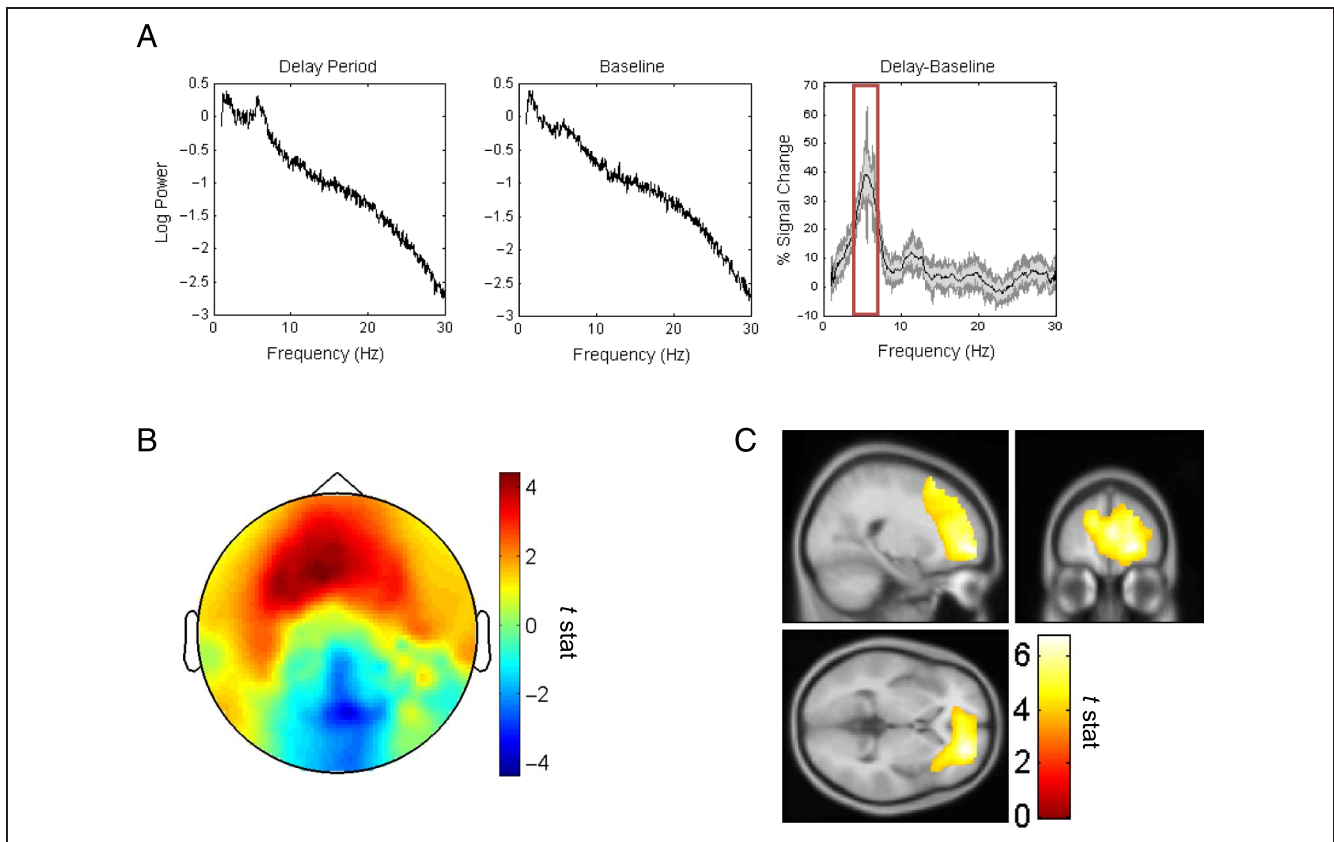
**Figure 3.** Delay versus baseline period, 4- to 7-Hz theta power changes. (A) Power spectra from a virtual electrode placed in the frontal midline region identified by a previous study ($x = 0$, $y = 58$, $z = 22$; Kaplan et al., 2014) for the delay and baseline periods as well as the difference in power between the two, averaged across all trials and participants. The power difference plot shows mean $\pm$ *SEM* across participants in gray. The power difference spectra show a single prominent peak at ~5.5 Hz, and we focus our subsequent analyses on a 3-Hz frequency band centered on this peak (i.e., 4–7 Hz). (B) Scalp level delay versus baseline period, 4- to 7-Hz theta power changes, which show an increase across the frontal midline region. (C, left) mPFC ($x = 22$, $y = 50$, $z = 0$; $z$ score = 4.51; peak voxel FWE corrected for the whole-brain volume, $p = .012$) theta power changes between the baseline and delay periods. Image shown at $p < .001$ uncorrected and overlaid on the canonical Montreal Neurological Institute 152 T1 image.

no cortical regions showed greater theta power during baseline periods, compared with the delay period.

Given that changes in the 1- to 4-Hz delta/low theta band have also been associated with human mnemonic function (Jacobs, 2014; Watrous, Lee, et al., 2013), we used the LCMV beamformer algorithm to assay changes in 1- to 4-Hz power between the baseline and delay periods across the whole brain. We observed a single subthreshold peak in the left insula that did not survive FWE correction for multiple comparisons. Notably, however, no significant changes were observed in the frontal lobe or MTL (data not shown).
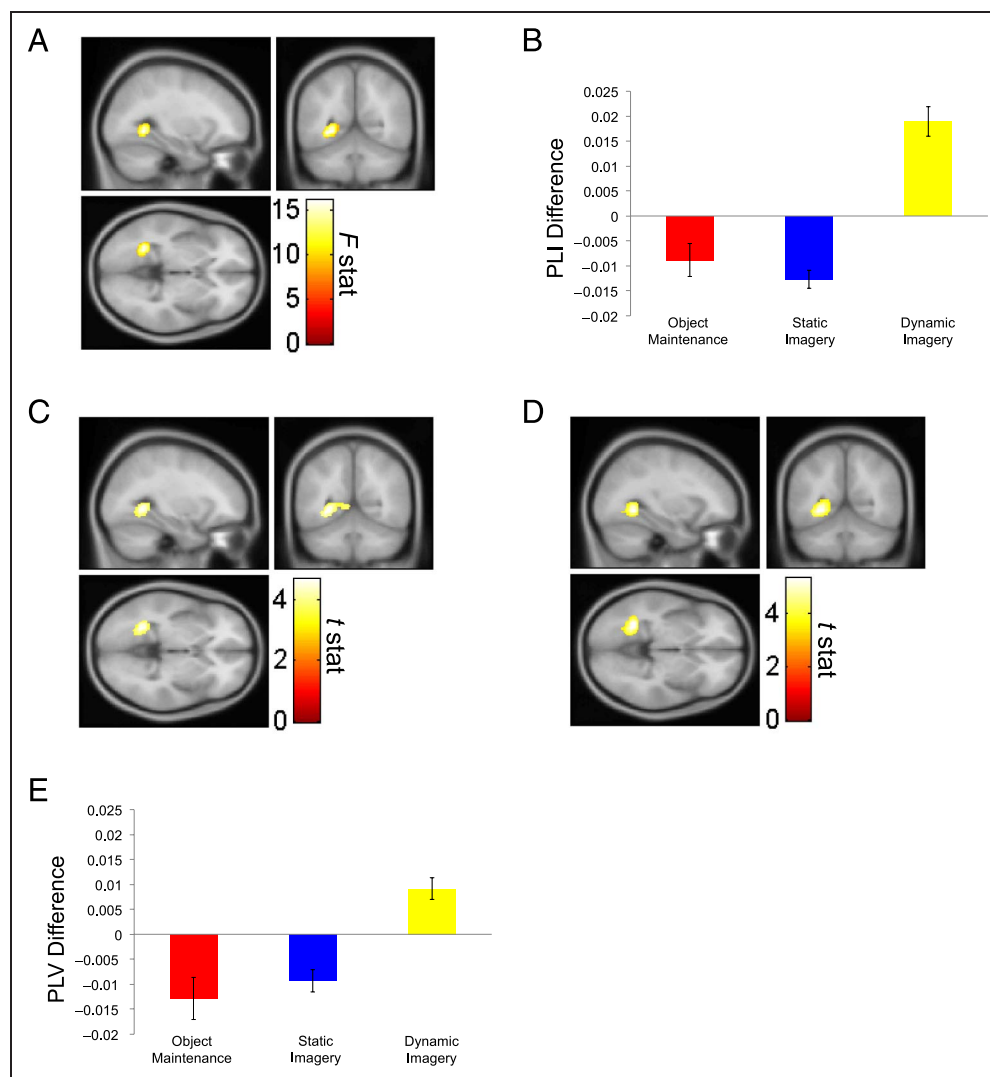
## Theta Phase Coupling

Next, we used the mPFC region that exhibited a significant theta power increase between the baseline and delay periods as a seed region to investigate changes in theta phase coupling across the whole brain. As in a previous study (Kaplan et al., 2014), the specific seed voxel for each participant was chosen as that with the greatest theta power increase between the baseline and delay periods within 20 mm of the group maximum, to account

for variance in frontal midline theta source locations between participants (Isihara et al., 1981).

First, we used the PLI (Stam et al., 2007; see Methods), a technique that eliminates volume conduction effects, to look for increases in theta phase coupling between the mPFC seed region and all other voxels in the brain. After correcting for eye movements and oscillatory power in seed and source voxels, we found no significant increases in theta phase coupling with the mPFC anywhere in the brain between the delay and baseline periods averaged over all three conditions.

We then compared mPFC theta coupling differences between the three conditions using a $1 \times 3$ within-participant repeated-measures ANOVA. In a whole-brain analysis, the most significant main effect of Condition on mPFC phase coupling was found in the left posterior MTL extending into the RSc ($x = -28$, $y = -54$, $z = -2$; $z$ score = 4.13, $F(2, 30) = 16.1$; peak voxel FWE bilateral MTL SVC, $p = .011$; Figure 4A). Subsequent $t$ tests indicated that mPFC–MTL/RSc theta phase coupling was significantly higher for dynamic imagery than both object maintenance ($x = -28$, $y = -54$, $z = -2$; $t(15) = 4.60$; $z$ score = 3.97;

**Figure 4.** Delay period 4- to 7-Hz mPFC theta phase coupling; PLI whole-brain analysis. (A) 1 × 3 interaction between Object maintenance, Static imagery, and Dynamic imagery for mPFC theta phase coupling, showing a significant cluster in the left posterior MTL ($x = -28$, $y = -54$, $z = -2$; $z$ score = 4.13; peak voxel FWE for bilateral MTL, $p = .011$) extending into the RSc. (B) Mean mPFC PLI with 10-mm sphere around the left posterior MTL peak voxel ($x = -28$, $y = -54$, $z = -2$) for all three conditions versus baseline. (C) mPFC theta phase coupling for dynamic imagery versus object maintenance, showing a significant cluster in the left posterior MTL ($x = -28$, $y = -54$, $z = -2$; $z$ score = 3.97; peak voxel FWE for bilateral MTL, $p = .016$), extending into the RSc. (D) mPFC theta phase coupling for dynamic imagery versus static imagery, showing a significant cluster in the left posterior MTL ($x = -30$, $y = -54$, $z = -4$; $z$ score = 4.45; peak voxel FWE corrected for whole-brain volume, $p = .03$), extending into the RSc. All images shown at $p < .001$ uncorrected for visualization purposes and overlaid on the canonical Montreal Neurological Institute 152 T1 image. (E) Mean mPFC PLV with 10-mm sphere around the left posterior MTL peak PLI voxel in A for all three conditions versus baseline. All bar graphs show mean ± *SEM* over the 16 participants.



peak voxel FWE SVC, $p = .016$; Figure 4C) and static imagery ($x = -30$, $y = -54$, $z = -4$; $t(15) = 5.35$, $z$ score = 4.45; peak voxel FWE whole-brain corrected, $p = .03$; Figure 4D).

To corroborate these findings, we made use of a more sensitive measure of phase coupling—the PLV (Lachaux et al., 1999; see Methods). We examined mPFC theta PLV within a 10-mm spherical ROI around the MTL/RSc peak voxel ($x = -28$, $y = -54$, $z = -2$) that displayed the most significant PLI difference between the three conditions above. Using a 1 × 3 repeated-measures ANOVA, we observed the same main effect of Condition ($F(2, 30) = 10.9$, $p = .001$). Subsequent paired $t$ tests revealed that dynamic imagery PLV was significantly higher than both static imagery ($t(15) = 4.07$, $p = .001$) and object maintenance ($t(15) = 3.54$, $p = .003$) within this region.

As with the PLI analysis, we did not observe any significant differences in PLV between the static imagery and object maintenance conditions ($p > .05$).

Investigating possible MTL lateralization during dynamic imagery, we found no significant difference in mPFC theta coupling with left versus right posterior MTL during dynamic imagery when we compared PLI values in the left MTL region that showed a significant increase during dynamic imagery effect with those from the right MTL region ($x = 48$, $y = -36$, $z = -10$; $t(15) = 4.75$, $z$ score = 3.67) that was most strongly coupled to the mPFC between the baseline and delay periods. Crucially, we did not identify any other significant differences in theta phase coupling between mPFC and any other brain regions or between any other conditions.

To ascertain whether mPFC–posterior MTL theta phase coupling difference between conditions related to differences in performance measures across conditions, we tested whether the mPFC–posterior MTL theta PLI values across all delay period trials correlated with our four behavioral regressors across trials. Using a 10-mm sphere around the left posterior MTL PLI peak, we found no significant correlations (all $ps > .05$) with any of the four behavioral regressors: memory performance, RT, subjective memory, and vividness ratings. Finally, we investigated whether mPFC mean PLI differences between the delay and baseline periods in any other brain regions correlated with any of these performance measures across trials but did not identify any significant effects.

## DISCUSSION

We have identified an increase in mPFC and anterior temporal lobe/MTL theta power during eyes-closed mental imagery of previously learned object sequences during a spatial working memory delay period compared with a preceding baseline period of eyes-closed rest. We found that the mPFC theta rhythm showed significantly stronger coupling with the left posterior MTL/RSc than any other brain region during imagined movement around learned object locations (dynamic imagery), compared with static imagery of learned object sequences in a scene (static imagery) or over a blank background (object maintenance).

Our theta power findings add to a rich literature of human working memory studies exploring theta oscillations in the frontal midline during the delay period of human working memory tasks (see Hsieh & Ranganath, 2014, for a review). We found increased mPFC theta power for mental imagery during a working memory delay period before retrieval, versus a baseline period, which parallels results from a previous MEG study that found increased mPFC theta during cued retrieval of previously learned spatial representations (Kaplan et al., 2014). Furthermore, similar to previous MEG and intracranial EEG studies, we also observed increased MTL theta power during a working memory delay period (Poch, Fuentemilla, Barnes, & Duzel, 2011; Axmacher et al., 2010; Cashdollar et al., 2009; Raghavachari et al., 2006; Tesche & Karhu, 2000). Frontal midline theta is often linked to directed attention (Ishii et al., 1999, 2014; see review by Mitchell, McNaughton, Flanagan, & Kirk, 2008), which we did not directly measure in this task. However, if there were any differences in directed attention between conditions, they did not cause any observable differences in frontal midline theta power.

Specifically, comparable with our findings, a previous study observed increased delay period mPFC and hippocampal theta power during spatial integration of object locations (Olsen, Rondina, Riggs, Meltzer, & Ryan, 2013). Unlike the study by Olsen and colleagues, we did not observe separate theta sources in the mPFC

and hippocampus during the delay period. This discrepancy might be a consequence of the relatively small number of trials and participants in our task, which increase the difficulty of estimating deep sources with MEG (Quraan, Moses, Hung, Mills, & Taylor, 2011; also see Dalal et al., 2013, for evidence relating direct human hippocampal recordings to MEG source reconstruction). In addition, EEG studies have seen increased frontal midline theta oscillations corresponding to the maintenance of the serial position of items (Hsieh, Ekstrom, & Ranganath, 2011), both spatial location and temporal order judgments (Roberts, Hsieh, & Ranganath, 2013), and the number of items being maintained in working memory (Jensen & Tesche, 2002). These results allow for the possibility that the frontal midline theta rhythm might provide top–down control to maintain the serial order or relation between previously learned spatial or temporal hippocampal representations before retrieval (Olsen et al., 2013), which in the case of our spatial imagery task, would also require MTL/parietal regions related to processing different viewpoints (Byrne et al., 2007).

The mPFC delay period theta rhythm was more strongly coupled to the posterior MTL than any other brain region, further emphasizing the importance of mPFC–MTL theta phase coupling during mnemonic tasks (Backus, Schoffelen, Szebényi, Hanslmayr, & Doeller, 2016; Garrido, Barnes, Kumaran, Maguire, & Dolan, 2015; Fuentemilla et al., 2014; Kaplan et al., 2014; Guitart-Masip et al., 2013; Watrous, Tandon, et al., 2013; Anderson, Rajagovindan, Ghacibeh, Meador, & Ding, 2010). Although the mPFC–right posterior MTL phase coupling delay period effect did not significantly vary by condition, unlike the mPFC–left MTL theta coupling effect we observed, all delay period conditions were also above baseline.

Looking across the different imagery conditions revealed significant differences in mPFC theta phase coupling with the left posterior MTL/RSc according to condition. Crucially, mPFC–MTL/RSc theta coupling was higher for dynamic spatial imagery than our other two delay period imagery manipulations, and the mPFC theta rhythm displayed no significant 4- to 7-Hz phase locking with any other brain region. We also found that mPFC–MTL theta coupling did not show any effect of hemispheric lateralization for dynamic imagery, because there was no significant mPFC theta coupling with the left or right MTL during dynamic imagery. Crucially, no behavioral rating correlated with mPFC–pMTL/RSc theta coupling among the three conditions, suggesting that the increase in mPFC–pMTL/RSc theta coupling for dynamic imagery was due to specific condition demands (e.g., mental imagery for multiple viewpoints, dynamically changing scenes) rather than differences in general behavioral performance (e.g., memory strength). Similar to past studies of spatial attention in human electrophysiology (Mangun & Hillyard, 1990), future experiments should investigate the relationships between distributed neural responses at different stages of dynamic spatial

imagery and measures of performance or vividness, to separate responses reflecting the types of processing involved from those reflecting successful execution of that processing type. Furthermore, human intracranial EEG recordings may be better suited than MEG studies to investigate the temporal dynamics of interregional phase interactions, and future studies can investigate the potentially rich, temporal phase coupling dynamics that might differ between imagery conditions.

Notably, one intracranial EEG study recording from human MTL and RSc (Foster et al., 2013) found increased theta phase coupling between the two regions during autobiographical memory, an effect that might be due to the increased dynamic imagery demands of the task. Taken together, these findings complement a previous hypothesis that theta synchronization between MTL/RSc and mPFC should accompany increased contextual associations (Aminoff, Kveraga, & Bar, 2013). Both the posterior MTL and RSc are thought to encode different viewpoints into a large-scale understanding of an environment (Vass & Epstein, 2013).

In terms of specific neural mechanisms, the finding of mPFC–MTL/RSc theta synchrony during dynamic imagery (i.e., movement of viewpoint) supports a recent model of spatial mental imagery. This model proposes that coherent spatial imagery results from a theta-rhythmic interaction between MTL and medial parietal areas, mediated by RSc (Byrne et al., 2007; Burgess et al., 2001). Within this model, pFC is hypothesized to control movements of viewpoint during mental exploration by modulating alternating temporal–parietal flows of information (Dhindsa et al., 2014).

Our findings illustrate the importance of mPFC–MTL interregional phase coupling in memory, irrespective of the presence or absence of theta power changes (Brincat & Miller, 2015; Watrous, Lee, et al., 2013). We provide further support to an expanding literature relating frequency-band-specific interregional phase coupling to a variety of cognitive processes (for reviews, see Fell & Axmacher, 2011; Jutras & Buffalo, 2010; Buzsáki, 2006; Fries, 2005). An important caveat to our findings is that our 4- to 7-Hz dynamic imagery effect is localized to the posterior MTL/RSc, not specifically to the hippocampus. Indeed, a lower frequency of ~1–4 Hz in the human hippocampus has been related to the hippocampal theta rhythm in rodents (Jacobs, 2014; Watrous et al., 2013), and we had no prediction about how other frontal midline or hippocampal theta rhythms might couple with other frequency bands in other neocortical regions, such as the alpha/beta band, that are present during memory formation (Hanslmayr, Staresina, & Bowman, 2016). Future models can investigate interregional interactions and potential oscillatory multiplexing (Ekstrom & Watrous, 2014; Watrous & Ekstrom, 2014) to better explore the mechanisms underlying dynamic imagery and memory formation.

Hippocampal–mPFC theta phase locking is also commonly observed during rodent spatial exploration and correlates with behavioral performance (Benchenane et al., 2010; Hyman, Zilli, Paley, & Hasselmo, 2010; Sigurdsson, Stark, Karayiorgou, Gogos, & Gordon, 2010; Jones & Wilson, 2005; see Colgin, 2011, and Gordon, 2011, for reviews). Notably, grid cell firing in the entorhinal cortex is also associated with theta states, and grid-like processing has been observed in medial prefrontal, parietal, and temporal regions (Doeller, Barry, & Burgess, 2010). Recent fMRI studies found grid-like processing in the MTL also during mental navigation (Bellmund, Deuker, Navarro Schröder, & Doeller, 2016; Horner, Bisby, Zotow, Bush, & Burgess, 2016), which parallels our dynamic versus static imagery results and suggests that both theta rhythmicity and spatial cell firing might play a role in the mental exploration of imagined spaces.

## Conclusions

Our findings suggest that theta oscillations in the mPFC and MTL could work in tandem, along with the RSc, to coordinate dynamic mental imagery during spatial working memory maintenance. Our results allow for the possibility that oscillatory interactions in the theta band between mPFC and MTL/RSc in humans could underlie the mental exploration of possible spatial trajectories and, more generally, mental simulation and fictive planning (Buzsáki & Moser, 2013; Byrne et al., 2007).

## REFERENCES

Aftanas, L. I., & Golocheikine, S. A. (2001). Human anterior and frontal midline theta and lower alpha reflect emotionally positive state and internalized attention: High-resolution EEG investigation of meditation. *Neuroscience Letters, 310,* 57–60.

Aminoff, E. M., Kveraga, K., & Bar, M. (2013). The role of the parahippocampal cortex in cognition. *Trends in Cognitive Sciences, 17,* 379–390.

Anderson, K. L., Rajagovindan, R., Ghacibeh, G. A., Meador, K. J., & Ding, M. (2010). Theta oscillations mediate interaction between prefrontal cortex and medial temporal lobe in human memory. *Cerebral Cortex, 20,* 1604–1612.

Axmacher, N., Henseler, M. M., Jensen, O., Weinrech, I., Elger, C. E., & Fell, J. (2010). Cross-frequency coupling supports multi-item working memory in the human hippocampus.

*Proceedings of the National Academy of Sciences, U.S.A., 107,* 3228–3233.

Backus, A. R., Schoffelen, J. M., Szebényi, S., Hanslmayr, S., & Doeller, C. F. (2016). Hippocampal-prefrontal theta oscillations support memory integration. *Current Biology, 26,* 450–457.

Banquet, J. P. (1973). Spectral analysis of the EEG in meditation. *Electroencephalography and Clinical Neurophysiology, 35,* 143–151.

Barnes, G. R., & Hillebrand, A. (2003). Statistical flattening of MEG beamformer images. *Human Brain Mapping, 18,* 1–12.

Battaglia, F. P., Benchenane, K., Sirota, A., Pennartz, C. M., & Wiener, S. I. (2011). The hippocampus: Hub of brain network communication for memory. *Trends in Cognitive Sciences, 15,* 310–318.

Bellmund, J. L., Deuker, L., Navarro Schröder, T., & Doeller, C. F. (2016). Grid-cell representations in mental simulation. *eLife, 5,* e17089.

Benchenane, K., Peyrache, A., Khamassi, M., Tierney, P. L., Gioanni, Y., Battaglia, F. P., et al. (2010). Coherent theta oscillations and reorganization of spike timing in the hippocampal network upon learning. *Neuron, 66,* 921–936.

Bird, C. M., & Burgess, N. (2008). The hippocampus and memory: Insights from spatial processing. *Nature Reviews Neuroscience, 9,* 182–194.

Brincat, S. L., & Miller, E. K. (2015). Frequency-specific hippocampal-prefrontal interactions during associative learning. *Nature Neuroscience, 18,* 576–581.

Burgess, N. (2006). Spatial memory: How egocentric and allocentric combine. *Trends in Cognitive Sciences, 10,* 551–557.

Burgess, N., Becker, S., King, J. A., & O'Keefe, J. (2001). Memory for events and their spatial context: Models and experiments. *Philosophical Transactions of the Royal Society of London, Series B, Biological Sciences, 356,* 1493–1503.

Burgess, N., Spiers, H. J., & Paleologou, E. (2004). Orientational manoeuvres in the dark: Dissociating allocentric and egocentric influences on spatial memory. *Cognition, 94,* 149–166.

Buzsáki, G. (2006). *Rhythms of the brain.* New York: Oxford University Press.

Buzsáki, G., & Moser, E. I. (2013). Memory, navigation and theta rhythm in the hippocampal-entorhinal system. *Nature Neuroscience, 16,* 130–138.

Byrne, P., Becker, S., & Burgess, N. (2007). Remembering the past and imagining the future: A neural model of spatial memory and imagery. *Psychological Review, 114,* 340–375.

Caplan, J. B., Madsen, J. R., Schulze-Bonhage, A., Aschenbrenner-Scheibe, R., Newman, E. L., & Kahana, M. J. (2003). Human theta oscillations related to sensorimotor integration and spatial learning. *Journal of Neuroscience, 23,* 4726–4736.

Cashdollar, N., Malecki, U., Rugg-Gunn, F. J., Duncan, J. S., Lavie, N., & Duzel, E. (2009). Hippocampus-dependent and -independent theta-networks of active maintenance. *Proceedings of the National Academy of Sciences, U.S.A., 106,* 20493–20498.

Colgin, L. L. (2011). Oscillations and hippocampal-prefrontal synchrony. *Current Opinion in Neurobiology, 21,* 467–474.

Dalal, S. S., Jerbi, K., Bertrand, O., Adam, C., Ducorps, A., Schwartz, D., et al. (2013). Evidence for MEG detection of hippocampus oscillations and cortical gamma-band activity from simultaneous intracranial EEG. *Epilepsy and Behavior, 28,* 288–292.

Dhindsa, K., Drobinin, V., King, J., Hall, G. B., Burgess, N., & Becker, S. (2014). Examining the role of the temporo-parietal network in memory, imagery, and viewpoint transformations. *Frontiers in Human Neuroscience, 8,* 709.

Doeller, C. F., Barry, C., & Burgess, N. (2010). Evidence for grid cells in a human memory network. *Nature, 463,* 657–661.

Ekstrom, A. D., Caplan, J. B., Ho, E., Shattuck, K., Fried, I., & Kahana, M. J. (2005). Human hippocampal theta activity during virtual navigation. *Hippocampus, 15,* 881–889.

Ekstrom, A. D., & Watrous, A. J. (2014). Multifaceted roles for low-frequency oscillations in bottom–up and top–down processing during navigation and memory. *Neuroimage, 85,* 667–677.

Epstein, R. A. (2008). Parahippocampal and retrosplenial contributions to human spatial navigation. *Trends in Cognitive Sciences, 12,* 388–396.

Fell, J., & Axmacher, N. (2011). The role of phase synchronization in memory processes. *Nature Reviews Neuroscience, 12,* 105–118.

Foster, B. L., Kaveh, A., Dastjerdi, M., Miller, K. J., & Parvizi, J. (2013). Human retrosplenial cortex displays transient theta phase locking with medial temporal cortex prior to activation during autobiographical memory retrieval. *Journal of Neuroscience, 33,* 10439–10446.

Fries, P. (2005). A mechanism for cognitive dynamics: Neuronal communication through neuronal coherence. *Trends in Cognitive Sciences, 9,* 474–480.

Fuentemilla, L., Barnes, G. R., Duzel, E., & Levine, B. (2014). Theta oscillations orchestrate medial temporal lobe and neocortex in remembering autobiographical memories. *Neuroimage, 85,* 730–737.

Garrido, M. I., Barnes, G. R., Kumaran, D., Maguire, E. A., & Dolan, R. J. (2015). Ventromedial prefrontal cortex drives hippocampal theta oscillations induced by mismatch computations. *Neuroimage, 15,* 362–370.

Gordon, J. A. (2011). Oscillations and hippocampal-prefrontal synchrony. *Current Opinion in Neurobiology, 21,* 486–491.

Graziano, M., & Gross, C. (1993). A bimodal map of space: Somatosensory receptive fields in the macaque putamen with corresponding visual receptive fields. *Experimental Brain Research, 97,* 96–109.

Guitart-Masip, M., Barnes, G. R., Horner, A., Bauer, M., Dolan, R. J., & Duzel, E. (2013). Synchronization of medial temporal lobe and prefrontal rhythms in human decision making. *Journal of Neuroscience, 33,* 442–451.

Hanslmayr, S., Staresina, B. P., & Bowman, H. (2016). Oscillations and episodic memory: Addressing the synchronization/desynchronization conundrum. *Trends in Neurosciences, 39,* 16–25.

Hassabis, D., Kumaran, D., Vann, S. D., & Maguire, E. A. (2007). Patients with hippocampal amnesia cannot imagine new experiences. *Proceedings of the National Academy of Sciences, U.S.A., 104,* 1726–1731.

Henson, R. N., Mattout, J., Phillips, C., & Friston, K. J. (2009). Selecting forward models for MEG source-reconstruction using model-evidence. *Neuroimage, 46,* 168–176.

Horner, A. J., Bisby, J. A., Zotow, E., Bush, D., & Burgess, N. (2016). Grid-like processing of imagined navigation. *Current Biology, 26,* 842–847.

Hsieh, L. T., Ekstrom, A. D., & Ranganath, C. (2011). Neural oscillations associated with item and temporal order maintenance in working memory. *Journal of Neuroscience, 31,* 10803–10810.

Hsieh, L. T., & Ranganath, C. (2014). Frontal midline theta oscillations during working memory maintenance and episodic encoding and retrieval. *Neuroimage, 85,* 721–729.

Hyman, J. M., Zilli, E. A., Paley, A. M., & Hasselmo, M. E. (2010). Working memory performance correlates with prefrontal-hippocampal theta interactions but not with prefrontal neuron firing rates. *Frontiers in Integrative Neuroscience, 4,* 2.

Ishii, R., Canuet, L., Ishihara, T., Aoki, Y., Ikeda, S., Hata, M., et al. (2014). Frontal midline theta rhythm and gamma power changes during focused attention on mental calculation: An MEG beamformer analysis. *Frontiers in Human Neuroscience, 8,* 406.

Ishii, R., Shinosaki, K., Ukai, S., Inouye, T., Ishiahara, T., Yoshimine, T., et al. (1999). Medial prefrontal cortex generates frontal midline theta rhythm. *NeuroReport, 10,* 675–679.

Isihara, T., Hayashi, H., & Hishikawa, Y. (1981). Distribution of frontal midline theta rhythm (FmO) on the scalp in different states (mental calculation, resting and drowsiness). *Electroencephalography and Clinical Neurophysiology, 52,* S19.

Jacobs, J. (2014). Hippocampal theta oscillations are slower in humans than in rodents: Implications for models of spatial navigation and memory. *Philosophical Transactions of the Royal Society of London, Series B, Biological Sciences, 369,* 20130304.

Jensen, O., & Tesche, C. D. (2002). Frontal theta activity in humans increases with memory load in a working memory task. *European Journal of Neuroscience, 28,* 67–72.

Jones, M. W., & Wilson, M. A. (2005). Theta rhythms coordinate hippocampal-prefrontal interactions in a spatial memory task. *PLoS Biology, 3,* e402.

Jutras, M. J., & Buffalo, E. A. (2010). Synchronous neural activity and memory formation. *Current Opinion in Neurobiology, 20,* 150–155.

Kahana, M. J., Sekuler, R., Caplan, J. B., Kirschen, M., & Madsen, J. R. (1999). Human theta oscillations exhibit task dependence during virtual maze navigation. *Nature, 399,* 781–784.

Kaplan, R., Bush, D., Bonnefond, M., Bandettini, P. A., Barnes, G. R., Doeller, C. F., et al. (2014). Medial prefrontal phase coupling during spatial memory retrieval. *Hippocampus, 24,* 656–665.

Kaplan, R., Doeller, C. F., Barnes, G. R., Litvak, V., Düzel, E., Bandettini, P. A., et al. (2012). Movement-related theta rhythm in humans coordinating self-directed hippocampal learning. *PLoS Biology, 10,* e1001267.

Kiebel, S. J., & Friston, K. J. (2004a). Statistical parametric mapping for event-related potentials: 1. Generic considerations. *Neuroimage, 22,* 492–502.

Kiebel, S. J., & Friston, K. J. (2004b). Statistical parametric mapping for event-related potentials (II): A hierarchical temporal model. *Neuroimage, 22,* 503–520.

Kilner, J. M., Kiebel, S. J., & Friston, K. J. (2005). Applications of random field theory to electrophysiology. *Neuroscience Letters, 374,* 174–178.

Lachaux, J., Rodriguez, E., Martiniere, J., & Varela, F. (1999). Measuring phase synchrony in brain signals. *Human Brain Mapping, 8,* 194–208.

Lehmann, D., Henggeler, B., Koukkou, M., & Michel, C. M. (1993). Source localization of brain electric field frequency bands during conscious, spontaneous, visual imagery and abstract thought. *Brain Research, Cognitive Brain Research, 1,* 203–210.

Litvak, V., Mattout, J., Kiebel, S., Phillips, C., Henson, R., Kilner, J., et al. (2011). EEG and MEG data analysis in SPM8. *Computational Intelligence and Neuroscience, 2011,* 852961.

Mangun, G. R., & Hillyard, S. A. (1990). Allocation of visual attention to spatial locations: Tradeoff functions for event-related brain potentials and detection performance. *Perception & Psychophysics, 47,* 532–550.

Mitchell, D. J., McNaughton, N., Flanagan, D., & Kirk, I. J. (2008). Frontal-midline theta from the perspective of hippocampal "theta". *Progress in Neurobiology, 86,* 156–185.

Muthukumaraswamy, S. D., & Singh, K. D. (2011). A cautionary note on the interpretation of phase-locking estimates with concurrent changes in power. *Clinical Neurophysiology, 122,* 2324–2325.

Nolte, G. (2003). The magnetic lead field theorem in the quasi-static approximation and its use for magnetoencephalography forward calculation in realistic volume conductor. *Physics in Medicine and Biology, 48,* 3637–3652.

O'Keefe, J. (2006). Hippocampal neurophysiology in the behaving animal. In P. Andersen, R. M. Morris, D. G. Amaral, T. V. P. Bliss, & J. O'Keefe (Eds.), *The hippocampus book* (pp. 475–548). New York: Oxford University Press.

O'Keefe, J., & Nadel, L. (1978). *Hippocampus as a cognitive map*. New York: Oxford University Press.

Olsen, R. K., Rondina, R., II, Riggs, L., Meltzer, J. A., & Ryan, J. D. (2013). Hippocampal and neocortical oscillatory contributions to visuospatial binding and comparison. *Journal of Experimental Psychology: General, 142,* 1335–1345.

Oostenveld, R., Fries, P., Maris, E., & Schoffelen, J.-M. (2011). FieldTrip: Open source software for advanced analysis of MEG, EEG, and invasive electrophysiological data. *Computational Intelligence and Neuroscience, 2011,* 156869.

Poch, C., Fuentemilla, L., Barnes, G. R., & Duzel, E. (2011). Hippocampal theta-phase modulation of replay correlates with configural-relational short-term memory performance. *Journal of Neuroscience, 31,* 7038–7042.

Quraan, M. A., Moses, S. N., Hung, Y., Mills, T., & Taylor, M. J. (2011). Detection and localization of hippocampal activity using beamformers with MEG: A detailed investigation using simulations and empirical data. *Human Brain Mapping, 32,* 812–827.

Raghavachari, S., Lisman, J. E., Tully, M., Madsen, J. R., Bromfield, E. B., & Kahana, M. J. (2006). Theta oscillations in human cortex during a working-memory task: Evidence for local generators. *Journal of Neurophysiology, 95,* 1630–1638.

Roberts, B. M., Hsieh, L. T., & Ranganath, C. (2013). Oscillatory activity during maintenance of spatial and temporal information in working memory. *Neuropsychologia, 51,* 349–357.

Sasaki, K., Nambu, A., Tsujimoto, T., Matsuzaki, R., Kyuhou, S., & Gemba, H. (1996). Studies on integrative functions of the human frontal association cortex with MEG. *Cognitive Brain Research, 5,* 165–174.

Schacter, D. L., & Addis, D. R. (2007). The cognitive neuroscience of constructive memory: Remembering the past and imagining the future. *Philosophical Transactions of the Royal Society B, 362,* 773–786.

Schacter, D. L., Addis, D. R., Hassabis, D., Martin, V. C., Spreng, R. N., & Szpunar, K. K. (2012). The future of memory: Remembering, imagining, and the brain. *Neuron, 76,* 677–694.

Sigurdsson, T., Stark, K. L., Karayiorgou, M., Gogos, J. A., & Gordon, J. A. (2010). Impaired hippocampal-prefrontal synchrony in a genetic mouse model of schizophrenia. *Nature, 464,* 763–767.

Stam, C. J., Nolte, G., & Daffertshofer, A. (2007). Phase lag index: Assessment of functional connectivity from multi channel EEG and MEG with diminished bias from common sources. *Human Brain Mapping, 28,* 1178–1193.

Tesche, C. D., & Karhu, J. (2000). Theta oscillations index human hippocampal activation during a working memory task. *Proceedings of the National Academy of Sciences, U.S.A., 97,* 919–924.

Troebinger, L., Lopez, J. D., Lutti, A., Bradbury, D., Bestmann, S., & Barnes, G. (2014). High precision anatomy for MEG. *Neuroimage, 86,* 583–591.

Tzourio-Mazoyer, N., Landeau, B., Papathanassiou, D., Crivello, F., Etard, O., Delroix, N., et al. (2002). Automated anatomical labelling of activations in SPM using a macroscopic anatomical parcellation of the MNI MRI single-subject brain. *Neuroimage, 15,* 273–289.

Vanderwolf, C. H. (1969). Hippocampal electrical activity and voluntary movement in the rat. *Electroencephalography and Clinical Neurophysiology, 26,* 407–418.

Vass, L. K., & Epstein, R. A. (2013). Abstract representations of location and facing direction in the human brain. *Journal of Neuroscience, 33,* 6133–6142.

Wang, R. F., & Simons, D. J. (1999). Active and passive scene recognition across views. *Cognition, 70,* 191–210.

Wang, R. F., & Spelke, E. S. (2000). Updating egocentric representations in human navigation. *Cognition, 77,* 215–250.

Watrous, A. J., & Ekstrom, A. D. (2014). The spectro-contextual encoding and retrieval theory of episodic memory. *Frontiers in Human Neuroscience, 8,* 75.

Watrous, A. J., Lee, D. J., Izadi, A., Gurkoff, G. G., Shahlaie, K., & Ekstrom, A. D. (2013). A comparative study of human and rat hippocampal low-frequency oscillations during spatial navigation. *Hippocampus, 23,* 656–661.

Watrous, A. J., Tandon, N., Conner, C. R., Pieters, T., & Ekstrom, A. D. (2013). Frequency-specific network connectivity increases underlie accurate spatiotemporal memory retrieval. *Nature Neuroscience, 16,* 349–356.

Worsley, K. J., Marrett, S., Neelin, P., Vandal, A. C., Friston, K. J., & Evans, A. C. (1996). A unified statistical approach for determining significant signals in images of cerebral activation. *Human Brain Mapping, 4,* 58–73.

Worsley, K. J., Taylor, J. E., Tomaiuolo, F., & Lerch, J. (2004). Unified univariate and multivariate random field theory. *Neuroimage, 23(Suppl. 1),* S189–S195.